Engine Control

J.A. Cook[*], J.W. Grizzle[†], and J. Sun[*]

January 18, 1995

1 Introduction

Automotive engine control systems must satisfy diverse and often conflicting requirements. These include regulating exhaust emissions to meet increasingly stringent standards without sacrificing good drivability; providing increased fuel economy to satisfy customer desires and to comply with Corporate Average Fuel Economy (CAFE) regulations; and delivering these performance objectives at low cost, with the minimum set of sensors and actuators. The dramatic evolution in vehicle electronic control systems over the past two decades is substantially in response to the first of these requirements: It is the capacity and flexibility of microprocessor-based digital control systems, introduced in the 1970's to address the problem of emission control, which have resulted in the improved function and added convenience, safety and performance features that distinguish the modern automobile [8].

Although the problem of automotive engine control may encompass a number of different powerplants, the one with which this article is concerned is the ubiquitous four stroke cycle, spark ignition, internal combustion gasoline engine. Mechanically, this powerplant has remained essentially the same since Nikolaus Otto built the first successful example in 1876. In automotive applications, it consists most often of four, six or eight cylinders wherein reciprocating pistons transmit power via a simple connecting rod and crankshaft mechanism

[*] Ford Motor Company, Scientific Research Laboratory, Control Systems Department, Maildrop 1170 SRL, Dearborn, MI 48121-2053

[†] Department of EECS, Control Systems Laboratory, University of Michigan, Ann Arbor, MI 48109-2122; work supported in part by the National Science Foundation under contract NSF ECS-92-13551

to the wheels. Two complete revolutions of the crankshaft comprise the following sequence of operations: The initial 180 degrees of crankshaft revolution is the intake stroke, where the piston travels from top-dead-center (TDC) in the cylinder to bottom-dead-center (BDC). During this time an intake valve in the top of the cylinder is opened and a combustible mixture of air and fuel is drawn in from an intake manifold. Subsequent 180 degree increments of crankshaft revolution comprise the compression stroke, where the intake valve is closed and the mixture is compressed as the piston moves back to the top of the cylinder; the combustion stroke when, after the mixture is ignited by a spark plug, torque is generated at the crankshaft by the downward motion of the piston caused by the expanding gas; and finally, the exhaust stroke, when the piston moves back up in the cylinder, expelling the products of combustion through an exhaust valve. Three fundamental control tasks affect emissions, performance and fuel economy in the spark ignition engine: Air-fuel ratio control, that is, providing the correct ratio of air and fuel for efficient combustion to the proper cylinder at the right time; ignition control, which refers to firing the appropriate spark plug at the precise instant required; and control of exhaust gas recirculation to the combustion process to reduce the formation of oxide of nitrogen emissions.

1.1 Ignition Control

The spark plug is fired near the end of the compression stroke, as the piston approaches TDC. For any engine speed, the optimal time during the compression stroke for ignition to occur is the point at which the maximum brake torque (MBT) is generated. Spark timing significantly in advance of MBT risks damage from the piston moving against the expanding gas. As the ignition event is retarded from MBT, less combustion pressure is developed and more energy is lost to the exhaust stream. Numerous methods exist for energizing the spark plugs. For most of automotive history, cam activated breaker points were used to develop a high voltage in the secondary windings of an induction coil connected between the battery and a distributor. Inside the distributor, a rotating switch synchronized with the crankshaft

connected the coil to the appropriate spark plug. In the early days of motoring, the ignition system control function was accomplished by the driver who manipulated a lever located on the steering wheel to change ignition timing. A driver who neglected to retard the spark when attempting to start a hand cranked Model T Ford could suffer a broken arm if he experienced "kickback." Failing to advance the spark properly while driving resulted in less than optimal fuel economy and power. Before long, elaborate centrifugal and vacuum driven distributor systems were developed to adjust spark timing with respect to engine speed and torque. The first digital electronic engine control systems accomplished ignition timing simply by mimicking the functionality of their mechanical predecessors. Modern electronic ignition systems sense crankshaft position to provide accurate cycle-time information and may use barometric pressure, engine coolant temperature and throttle position along with engine speed and intake manifold pressure to schedule ignition events for the best fuel economy and drivability subject to emissions and spark knock constraints. Additionally, ignition timing may be used to modulate torque to improve transmission shift quality, and in a feedback loop as one control variable to regulate engine idle speed. In modern engines, the electronic control module activates the induction coil in response to the sensed timing and operating point information and, in concert with dedicated ignition electronics, routes the high voltage to the correct spark plug. One method of providing timing information to the control system is by using a magnetic proximity pick-up and a toothed wheel driven from the crankshaft to generate a square wave signal indicating TDC for successive cylinders. A signature pulse of unique duration is often used to establish a reference from which absolute timing can be determined. During the past ten years there has been substantial research and development interest in using in-cylinder piezoelectric or piezoresistive combustion pressure sensors for closed-loop feedback control of individual cylinder spark timing to MBT or to the knock limit. The advantages of combustion pressure based ignition control are reduced calibration and increased robustness to variability in manufacturing, environment, fuel, and due to component aging. The cost is in an increased sensor set and additional computing power.

1.2 Exhaust Gas Recirculation

Exhaust gas recirculation (EGR) systems were introduced as early as 1973 to control emissions of oxides of nitrogen (NOx). The principle of EGR is to reduce NOx formation during the combustion process by diluting the inducted air-fuel charge with inert exhaust gas. In electronically controlled EGR systems, this is accomplished using a metering orifice in the exhaust manifold to enable a portion of the exhaust gas to flow from the exhaust manifold through a vacuum actuated EGR control valve and into the intake manifold. Feedback based on the difference between the desired and measured pressure drop across the metering orifice is employed to duty cycle modulate a vacuum regulator controlling the EGR valve pintle position. Because manifold pressure rate and engine torque are directly influenced by EGR, the dynamics of the system can have a significant effect on engine response and, ultimately, vehicle drivability. Such dynamics are dominated by the valve chamber filling response time to changes in the EGR duty cycle command. The system can be represented as a pure transport delay associated with the time required to build up sufficient vacuum to overcome pintle shaft friction cascaded with first order dynamics incorporating a time constant which is a function of engine exhaust flow rate. Typically, the EGR control algorithm is a simple PI or PID loop. Nonetheless, careful control design is required to provide good emission control without sacrificing vehicle performance. An unconventional method to accomplish NOx control by exhaust recirculation is to directly manipulate the timing of the intake and exhaust valves. Variable cam timing (VCT) engines have demonstrated NOx control using mechanical and hydraulic actuators to adjust valve timing and affect the amount of internal EGR remaining in the cylinder after the exhaust stroke is completed. Early exhaust valve closing has the additional advantage that unburned hydrocarbons normally emitted to the exhaust stream are recycled through a second combustion event, reducing HC emissions as well. Although VCT engines eliminate the normal EGR system dynamics, the fundamentally multivariable nature of the resulting system presages a difficult engine control problem.

1.3 Air-Fuel Ratio Control

Historically, fuel control was accomplished by a carburetor which used a venturi arrangement and simple float and valve mechanism to meter the proper amount of fuel to the engine. For special operating conditions, such as idle or acceleration, additional mechanical and vacuum circuitry was required to assure satisfactory engine operation and good drivability. The demise of the carburetor was occasioned by the advent of three-way catalytic converters (TWC) for emission control. These devices simultaneously convert oxidizing (HC and CO) and reducing (NOx) species in the exhaust, but, as shown in Figure 1, require precise control of air-fuel ratio (A/F) to the stoichiometric value to be effective. Consequently, the electronic

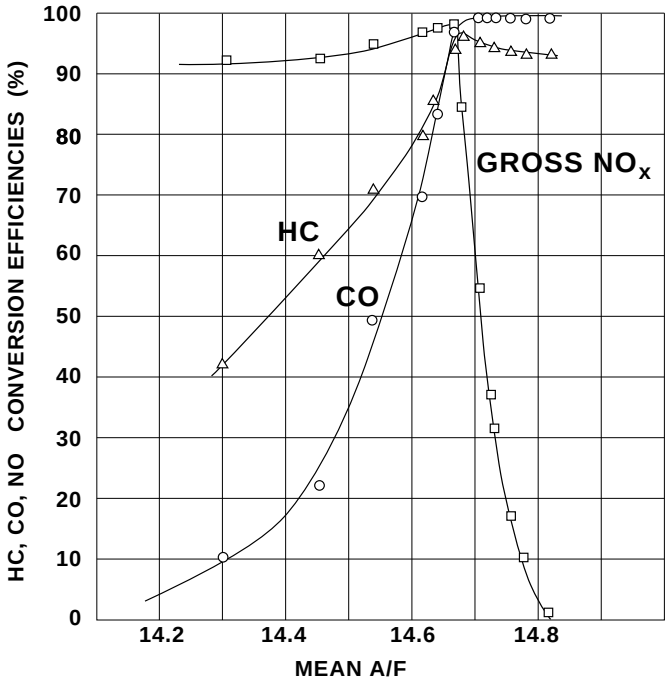

Figure 1: Typical TWC Efficiency Curves.

fuel system of a modern spark ignition automobile engine employs individual fuel injectors located in the inlet manifold runners close to the intake valves to deliver accurately timed and metered fuel to all cylinders. The injectors are regulated by an air-fuel ratio control system which has two primary components: a feedback portion in which a signal related to A/F from an exhaust gas oxygen (EGO) sensor is fed back through a digital controller

to regulate the pulse width command sent to the fuel injectors, and a feedforward portion in which injector fuel flow is adjusted in response to a signal from an air flow meter. The feedback, or closed-loop portion of the control system, is fully effective only under steady state conditions and when the EGO sensor has attained the proper operating temperature. The open-loop, or feedforward portion of the control system, is particularly important when the engine is cold (before the closed-loop A/F control is operational) and during transient operation (when the significant delay between the injection of fuel, usually during the exhaust stroke, just before the intake valve opens, and the appearance of a signal at the EGO sensor, possibly long after the conclusion of the exhaust stroke, inhibits good control). In Section 2.1, the open-loop A/F control problem will be examined with emphasis on accounting for sensor dynamics. The closed-loop problem will be addressed in Section 2.2 from a modern control systems perspective, where individual cylinder control of A/F is accomplished using a single EGO sensor.

1.4 Idle Speed Control

In addition to these essential tasks of controlling ignition, A/F and EGR, the typical on-board microprocessor performs many other diagnostic and control functions. These include electric fan control, purge control of the evaporative emissions canister, turbocharged engine wastegate control, overspeed control, electronic transmission shift scheduling and control, cruise control and idle speed control (ISC). The ISC requirement is to maintain constant engine RPM at closed throttle while rejecting disturbances such as automatic transmission neutral-to-drive transition, air conditioner compressor engagement and power steering lock-up. The idle speed problem is a difficult one, especially for small engines at low speeds where marginal torque reserve is available for disturbance rejection. The problem is made more challenging by the fact that significant parameter variation can be expected over the substantial range of environmental conditions in which the engine must operate. Finally, the idle speed control design is subject not only to quantitative performance requirements such

as overshoot and settling time, but also to more subjective measures of performance such as idle quality and the degree of noise and vibration communicated to the driver through the body structure. The idle speed control problem will be addressed in Section 3.

2 Air Fuel Ratio Control System Design

Due to the precipitous fall off of TWC efficiency away from stoichiometry, the primary objective of the A/F control system is to maintain the fuel metering in a stoichiometric proportion to the incoming air flow (the only exception to this occurs in heavy load situations where a rich mixture is required to avoid premature detonation (or knock) and keep the TWC from overheating). Variation in air flow commanded by the driver is treated as a disturbance to the system. A block diagram of the control structure is illustrated in Figure 2, and the two major subcomponents treated here are highlighted in bold. Subsection 2.1 describes

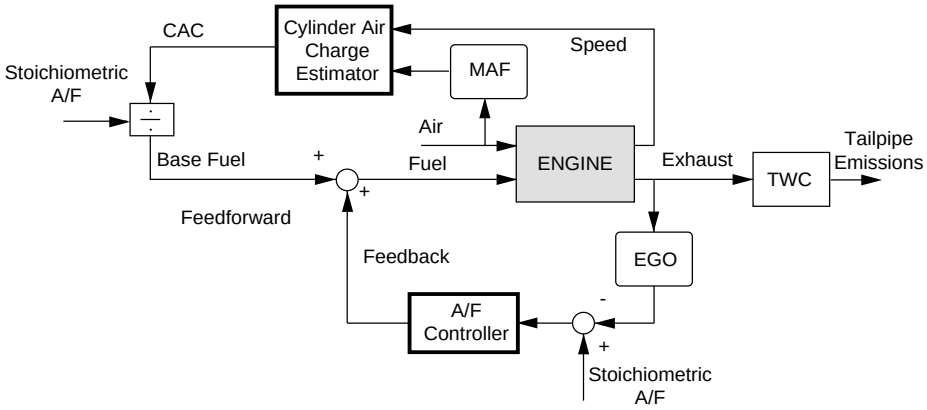

Figure 2: Basic A/F Control Loop Showing Major Feedforward and Feedback Elements.

the development and implementation of a cylinder air charge estimator for predicting the air charge entering the cylinders downstream of the intake manifold plenum on the basis of available measurements of air mass flow rate upstream of the throttle. The air charge estimate is used to form the base fuel calculation, which is often then modified to account for any fuel puddling dynamics and the delay associated with closed-valve fuel injection timing. Finally, a classical, time-invariant, single-input single-output (SISO) PI controller

is normally used to correct for any persistent errors in the open loop fuel calculation by adjusting the average A/F to perceived stoichiometry.

Even if the average A/F is controlled to stoichiometry, individual cylinders may be operating consistently rich or lean of the desired value. This cylinder-to-cylinder A/F maldistribution is due in part to injector variability. Consequently fuel injectors are machined to close tolerances to avoid individual cylinder flow discrepancies, resulting in high cost per injector. However, even if the injectors are perfectly matched, maldistribution can arise from individual cylinders having different breathing characteristics due to a combination of factors such as intake manifold configuration and valve characteristics. It is known that such A/F maldistribution can result in increased emissions due to shifts in the closed-loop A/F setpoint relative to the TWC [9]. Subsection 2.2 describes the development of a non-classical, periodically time-varying controller for tuning the A/F in each cylinder to eliminate this maldistribution.

Hardware Assumptions: The modeling and control methods presented here are applicable to just about any fuel injected engine. For illustration purposes only, it is assumed that the engine is a port fuel injected V8 with independent fuel control for each bank of cylinders. The cylinders are numbered one through four, starting from the front of the right bank, and five through 8, starting from the front of the left bank. The firing order of the engine is 1-3-7-2-6-5-4-8, which is not symmetric from bank to bank. Fuel injection is timed to occur on a closed valve prior to the intake stroke (induction event). For the purpose of closed-loop control, the engine is equipped with a switching-type EGO sensor located at the confluence of the individual exhaust runners, and just upstream of the catalytic converter. Such sensors typically incorporate a ZrO_2 ceramic thimble employing a platinum catalyst on the exterior surface to equilibrate the exhaust gas mixture. The interior surface of the sensor is exposed to the atmosphere. The output voltage is exponentially related to the ratio of O_2 partial pressures across the ceramic, and thus the sensor is essentially a switching device indicating by its state whether the exhaust gas is rich or lean of stoichiometry.

2.1 Cylinder Air Charge Computation

This subsection describes the development and implementation of an air charge estimator for an eight cylinder engine. A very real practical problem is posed by the fact that the hot-wire anemometers currently used to measure mass air flow rate have relatively slow dynamics. Indeed, the time constant of this sensor is often on the order of an induction event for an engine speed of 1500 revolutions per minute, and is only about four to five times faster than the dynamics of the intake manifold. Taking these dynamics into account in the air charge estimation algorithm can significantly improve the accuracy of the algorithm and have substantial benefits for reducing emissions.

2.1.1 Basic model

The air path of a typical engine is depicted in Figure 3. An associated lumped parameter phenomenological model suitable for developing an on-line cylinder air charge estimator [2] is now described. Let P, V, T and m be the pressure in the intake manifold (psi), volume of the intake manifold and runners (liters), temperature (°R) and mass (lbm) of the air in the intake manifold, respectively. Invoking the ideal gas law, and assuming that the manifold air temperature is slowly varying leads to

$$\frac{d}{dt}P = \frac{RT}{V}[MAF_a - \mathrm{C}yl(N, P, T_{EC}, T_i)], \tag{2.1}$$

where, MAF_a is the actual mass air flow metered in by the throttle, R is the molar gas constant, $Cyl(N, P, T_{EC}, T_i)$ is the average instantaneous air flow pumped out of the intake manifold by the cylinders, as a function of engine speed, N (RPM), manifold pressure, engine coolant temperature, T_{EC} (^oR), and air inlet temperature, T_i (^oR). It is assumed that both MAF_a and $Cyl(N, P, T_{EC}, T_i)$ have units of lbm/sec.

The dependence of the cylinder pumping or induction function on variations of the engine coolant and air inlet temperatures is modeled empirically by [10], page 187, as

$$Cyl(N, P, T_{EC}, T_i) = \mathrm{C}yl(N, P)\sqrt{\frac{T_i}{T_i^{\mathrm{mapping}}}}\,\frac{T_{EC}^{\mathrm{mapping}} + 2460}{T_{EC} + 2460}, \tag{2.2}$$

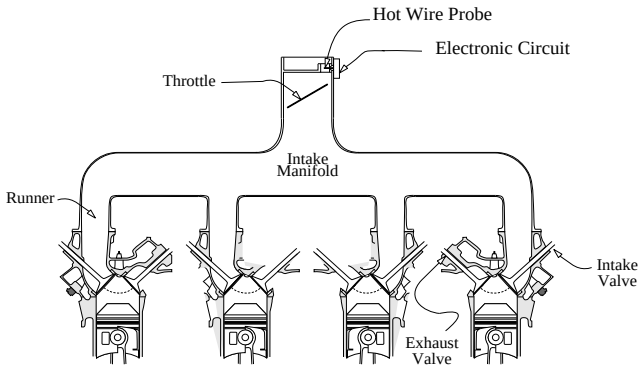

Figure 3: Schematic of Air Path in Engine.

where the superscript 'mapping' denotes the corresponding temperatures (^oR) at which the function $Cyl(N, P)$ is determined, based on engine mapping data. An explicit procedure for determining this function is explained in Subsection 2.1.2.

Cylinder air charge per induction event, CAC, can be determined directly from (2.1). In steady state, the integral of the mass flow rate of air pumped out of the intake manifold over two engine revolutions, divided by the number of cylinders, is the air charge per cylinder. Since engine speed is nearly constant over a single induction event, and the time in seconds for two engine revolutions is $\frac{120}{N}$, a good approximation of the inducted air charge on a per cylinder basis is given by

$$CAC = \frac{120}{nN} \mathrm{C}yl(N, P, T_{EC}, T_i) \text{ lbm}, \tag{2.3}$$

where n is the number of cylinders.

The final element to be incorporated in the model is the mass air flow meter. The importance of including this was demonstrated in [2]. For the purpose of achieving rapid on-line computations, a simple first order model will be used:

$$\gamma \frac{d}{dt} MAF_m + MAF_m = MAF_a \ , \tag{2.4}$$

where MAF_m is the measured mass air flow and γ is the time constant of the air meter. Substituting the left hand side of (2.4) for MAF_a in (2.1) yields

$$\frac{d}{dt} P = \frac{RT}{V} \left[\gamma \frac{d}{dt} MAF_m + MAF_m - \mathrm{C}yl(N, P, T_{EC}, T_i) \right] \tag{2.5}$$

To eliminate the derivative of MAF_m in the above equation, let $x = P - \gamma\frac{RT}{V}MAF_m$. This yields

$$\frac{d}{dt}x = \frac{RT}{V}\left[MAF_m - \mathrm{C}yl(N, x + \gamma\frac{RT}{V}MAF_m, T_{EC}, T_i)\right]. \tag{2.6}$$

Cylinder air charge is then computed from (2.3) as

$$CAC = \frac{120}{nN}\mathrm{C}yl(N, x + \gamma\frac{RT}{V}MAF_m, T_{EC}, T_i)\ . \tag{2.7}$$

Note that the effect of including the mass air flow meter's dynamics is to add a feedforward term involving the mass air flow rate to the cylinder air charge computation. When $\gamma = 0$, (2.6) and (2.7) reduce to an estimator which ignores the air meter's dynamics, or equivalently, treats the sensor as being infinitely fast.

2.1.2 Determining Model Parameters

The pumping function $\mathrm{C}yl(N, P)$ can be determined on the basis of steady-state engine mapping data. Equip the engine with a high bandwidth manifold absolute pressure sensor and exercise the engine over the full range of speed and load conditions, while recording the steady-state value of the instantaneous mass air flow rate as a function of engine speed and manifold pressure. For this purpose, any external exhaust gas recirculation should be disabled. A typical data set should cover every 500 RPM of engine speed from 500 to 5,000 RPM and every half psi of manifold pressure from 3 psi to atmosphere. For the purpose of making these measurements, it is preferable to use a laminar air flow element as this will in addition allow the calibration of the mass air flow meter to be verified. Record the engine coolant and air inlet temperatures for use in (2.2). The function $\mathrm{C}yl(N, P)$ can be represented as a table look-up or as a polynomial regressed against the above mapping data. In either case, it is common to represent it in the following functional form:

$$\mathrm{C}yl(N, P) = \mu(N)P + \beta(N). \tag{2.8}$$

The time constant of the air meter is best determined by installing the meter on a flow bench and applying step or rapid sinusoidal variations in air flow to the meter. Methods

for fitting an approximate first order model to the data can be found in any textbook on classical control. A typical value is $\gamma = 20$ms. Though not highly recommended, a value for the time constant can be determined by on-vehicle calibration, if an accurate determination of the pumping function has been completed. This is explained at the end of Subsection 2.1.3.

2.1.3 Model Discretization and Validation

The estimator (2.6) and (2.7) must be discretized for implementation. In engine models, an event based sampling scheme is often used [7]. For illustration purposes, the discretization will be carried out here for a V8; the modifications required for other configurations will be evident. Let k be the recursion index and let Δt_k be the elapsed time in seconds per 45 degrees of crank-angle advancement, or $\frac{1}{8}$ revolution; that is, $\Delta t_k = \frac{7.5}{N_k}$ sec., where N_k is the current engine speed in RPM. Then (2.6) can be Euler integrated as

$$x_k = x_{k-1} + \Delta t_k \frac{RT_{k-1}}{V}\left[MAF_{m,k-1} - Cyl(N_{k-1}, x_{k-1} + \gamma\frac{RT_{k-1}}{V}MAF_{m,k-1}, T_{EC}, T_i)\right] \quad (2.9)$$

The cylinder air charge is calculated by

$$CAC_k = 2\Delta t_k \mathrm{C}yl(N_k, x_k + \gamma\frac{RT_k}{V}MAF_{m,k}, T_{EC}, T_i) \ , \quad (2.10)$$

and need only be computed once per 90 crank-angle degrees.

The accuracy of the cylinder air charge model can be easily validated on an engine dynamometer equipped to maintain constant engine speed. Apply very rapid throttle tip-ins and tip-outs as in Figure 4, while holding the engine speed constant. If the model parameters have been properly determined, the calculated manifold pressure will accurately track the measured manifold pressure. Figure 5 illustrates one such test at 1500 RPM. The dynamic responses of the measured and computed values match up quite well. There is some inaccuracy in the quasi-steady state values at 12 psi; this corresponds to an error in the pumping function $Cyl(N, P)$ at high manifold pressures, so, in this operating condition, it should be re-evaluated.

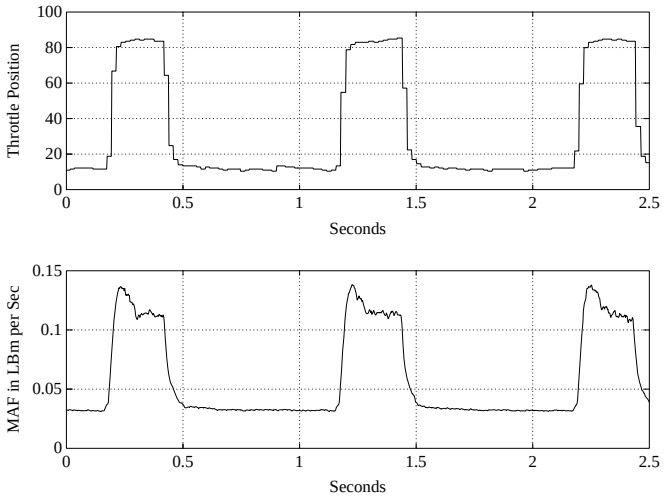

Figure 4: Engine Operating Conditions at Nominal 1500 RPM.

From Figure 5, it can be seen that the air meter time constant has been accurately identified in this test. If the value for γ in (2.4) had been chosen too large, then the computed manifold pressure would be leading the measured manifold pressure; conversely, if γ were too small, the computed value would lag the measured value.

2.2 Eliminating A/F Maldistribution through Feedback Control

Air-fuel ratio maldistribution is evidenced by very rapid switching of the EGO sensor on an engine-event-by-engine-event basis. Such cylinder-to-cylinder A/F maldistribution can result in increased emissions due to shifts in the closed loop A/F setpoint relative to the TWC [9]. The trivial control solution which consists of placing individual EGO sensors in each exhaust runner and wrapping independent PI controllers around each injector-sensor pair is not acceptable from an economic point of view; technically, there would also be problems due to the non-equilibrium condition of the exhaust gas immediately upon exiting the cylinder. This subsection details the development of a controller which eliminates A/F maldistribution on the basis of a single EGO sensor per engine bank. The controller is developed for the left bank of the engine.

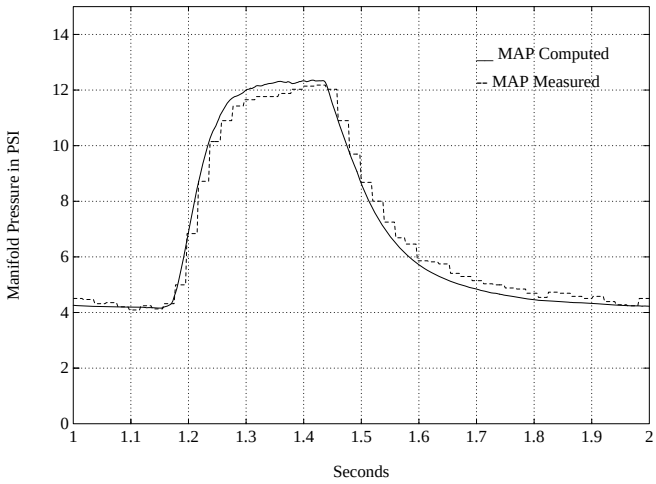

Figure 5: Comparison of Measured and Computed Manifold Pressure.

2.2.1 Basic Model

A control oriented, block diagram model for the A/F system of the left bank of an eight-cylinder engine is depicted in Figure 6. The model evolves at an engine speed-dependent sampling interval of 90 crank-angle degrees consistent with the 8-cylinder geometry (one exhaust event occurs every 90 degrees of crankshaft rotation). The engine is represented by injector gains G1 through G8, and pure delay z^{-d}, which accounts for the number of engine events that occur from the time that an individual cylinder's fuel injector pulse-width is computed until the corresponding exhaust valve opens to admit the mixture to the exhaust manifold. The transfer function H(z) represents the mixing process of the exhaust gases from the individual exhaust ports to the EGO sensor location, including any transport delay. The switching-type EGO sensor is represented by a first order transfer function followed by a preload (switch) nonlinearity.

Note that only cylinders 5 through 8 are inputs to the mixing model, H(z). This is due to the fact that the separate banks of the V8 engine are controlled independently. The gains and delays for cylinders 1 through 4 correspond to the right bank of the engine and are included in the diagram only to represent the firing order. Note furthermore that cylinders 5 and 6

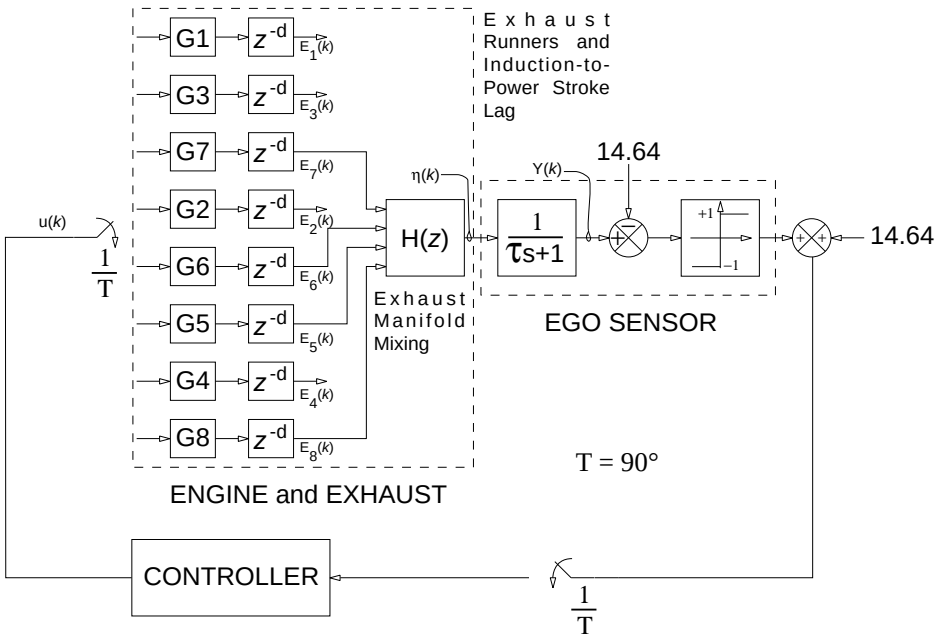

Figure 6: Control Oriented Block Diagram of A/F Subsystem.

exhaust within 90 degrees of one another, whereas cylinders 7 and 8 exhaust 270 degrees apart. Since the exhaust stroke of cylinder 6 is not complete before the exhaust stroke of cylinder 5 commences, for any exhaust manifold configuration, there will be mixing of the exhaust gases from these cylinders at the point where the EGO sensor samples the exhaust gas. We will adopt the notation that the sampling index, k, is a multiple of 90 degrees, that is, $x(k)$ is the quantity x at $k \cdot 90$ degrees; moreover, if we are looking at a signal's value during a particular point of an engine cycle, then we will denote this by $x(8k + j)$, which is x at $(8k + j) \cdot 90$ degrees, or, x at the j-th event of the k-th engine cycle. The initial time will be taken as $k = 0$ at top dead center (TDC) of the compression stroke of cylinder 1. The basic model for a V-6 or a four cylinder engine is simpler; see [3].

A dynamic model of the exhaust manifold mixing is difficult to determine with current technology. This is because a linear A/F measurement is required, and, currently, such sensors have a slow dynamic response in comparison with the time duration of an individual cylinder event. Hence, standard system identification methods break down. In [6], a model structure for the mixing dynamics and an attendant model parameter identification

procedure, compatible with existing laboratory sensors, is provided. This is outlined next.

The key assumption used to develop a mathematical model of the exhaust gas mixing is that once the exhaust gas from any particular cylinder reaches the EGO sensor, the exhaust of that cylinder from the previous cycle (two revolutions) has been completely evacuated from the exhaust manifold. It is further assumed that the transport lag from the exhaust port of

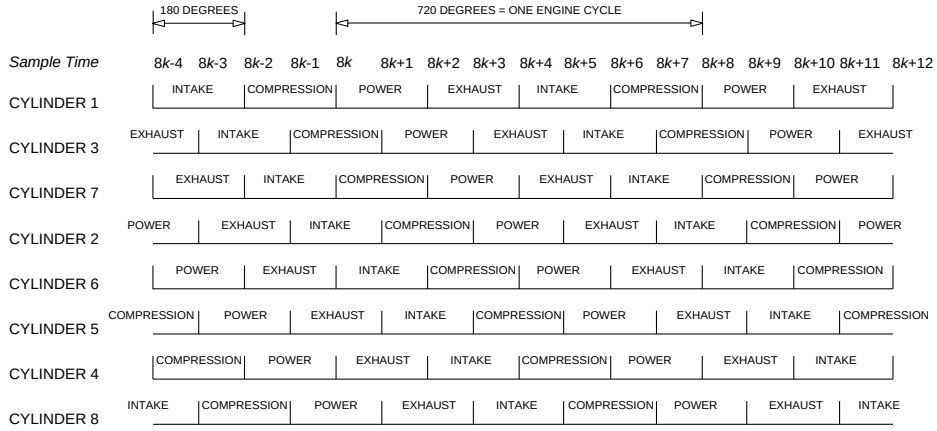

Figure 7: Timing Diagram for 8-Cylinder Engine

any cylinder to the sensor location is less than two engine cycles. With these assumptions, and with reference to the timing diagram of Figure 7, a model for the exhaust mixing dynamics may be expressed as relating the A/F at the sensor over one 720 crank-angle degree period beginning at $(8k)$ as a linear combination of the air-fuel ratios admitted to the exhaust manifold by cylinder 5 during the exhaust strokes occurring at times $(8k{+}7)$, $(8k\text{-}1)$ and $(8k\text{-}9)$; by cylinder 6 at $(8k{+}6)$, $(8k\text{-}2)$ and $(8k\text{-}10)$; by cylinder 7 at $(8k{+}4)$, $(8k\text{-}4)$ and $(8k\text{-}12)$; and by cylinder 8 at $(8k{+}1)$, $(8k\text{-}7)$ and $(8k\text{-}15)$. This relationship is given by

$$\begin{bmatrix} \eta(8k) \\ \eta(8k+1) \\ \vdots \\ \eta(8k+6) \\ \eta(8k+7) \end{bmatrix} = \begin{bmatrix} a_5(1,0) & \dots & a_8(1,0) \\ \vdots & & \\ a_5(8,0) & \dots & a_8(8,0) \end{bmatrix} \begin{bmatrix} E_5(8k+7) \\ E_6(8k+6) \\ E_7(8k+4) \\ E_8(8k+1) \end{bmatrix} + \begin{bmatrix} a_5(1,1) & \dots & a_8(1,1) \\ \vdots & & \\ a_5(8,1) & \dots & a_8(8,1) \end{bmatrix} \begin{bmatrix} E_5(8k-1) \\ E_6(8k-2) \\ E_7(8k-4) \\ E_8(8k-7) \end{bmatrix} + \begin{bmatrix} a_5(1,2) & \dots & a_8(1,2) \\ \vdots & & \\ a_5(8,2) & \dots & a_8(8,2) \end{bmatrix} \begin{bmatrix} E_5(8k-9) \\ E_6(8k-10) \\ E_7(8k-12) \\ E_8(8k-15) \end{bmatrix} \tag{2.11}$$

where: η is the actual A/F at the production sensor location, E_n is the exhaust gas A/F from cylinder n ($n = 5, 6, 7, 8$), and a_n is the time dependent fraction of the exhaust gas from cylinder n contributing to the air fuel ratio at the sensor. It follows from the key assumption that only 32 of the 96 coefficients in equation (2.11) can be non-zero. Specifically, every triplet $\{a_n(k,0), a_n(k,1), a_n(k,2)\}$ has, at most, one non-zero element. This will be exploited in the model parameter identification procedure.

2.2.2 Determining Model Parameters

The pure delay z^{-d} is determined by the type of injection timing used (open or closed-valve), and does not vary with engine speed or load. A typical value for closed-valve injection timing is $d = 8$. The time constant of the EGO sensor is normally provided by the manufacturer; if not, it can be estimated by installing it directly in the exhaust runner of one of the cylinders and controlling the fuel pulse-width to cause a switch from rich to lean and then lean to rich. A typical average value of these two times is $\tau = 70$ms.

The first step towards identifying the parameters in the exhaust mixing model is to determine which one of the parameters $\{a_n(k,0), a_n(k,1), a_n(k,2)\}$ is the possibly non-zero element; this can be uniquely determined on the basis of the transport delay between the opening of the exhaust valve of each cylinder and the time of arrival of the corresponding exhaust gas pulse at the EGO sensor. The measurement of this delay is accomplished by installing the fast, switching type EGO sensor in the exhaust manifold in the production location and carefully balancing the A/F of each cylinder to the stoichiometric value. Then, apply a step change in A/F to each cylinder and observe the time delay. The results of a typical test are given in [6]. The transport delays will change as a function of engine speed and load and thus should be determined at several operating points. In addition, they may not be a multiple of 90 degrees. A practical method to account for these issues through a slightly more sophisticated sampling schedule is outlined in [3].

At steady state, equation (2.11) reduces to

$$\begin{bmatrix} \eta(8k) \\ \eta(8k+1) \\ \vdots \\ \eta(8k+6) \\ \eta(8k+7) \end{bmatrix} = A_{mix} \begin{bmatrix} E_5(8k-1) \\ E_6(8k-2) \\ E_7(8k-4) \\ E_8(8k+1) \end{bmatrix} \tag{2.12}$$

where

$$A_{mix} = \begin{bmatrix} \sum_{j=0}^{2} a_5(1,j) & \dots & \sum_{j=0}^{2} a_8(1,j) \\ \vdots & \dots & \vdots \\ \sum_{j=0}^{2} a_5(8,j) & \dots & \sum_{j=0}^{2} a_8(1,j) \end{bmatrix} \tag{2.13}$$

This leads to the second part of the parameter identification procedure in which the values of the summed coefficients of equation (2.12) may be identified from "steady- state" experiments performed with a linear EGO sensor installed in the production location. Then, knowing which of the coefficients is nonzero, equation (2.11) may be evaluated.

Install a linear EGO sensor in the production location. Then the measured A/F response, $y(k)$, to the sensor input, $\eta(k)$, is modeled by

$$\begin{aligned} w(k+1) &= \alpha w(k) + (1-\alpha)\eta(k) \\ y(k) &= w(k), \end{aligned} \tag{2.14}$$

where $\alpha = e^{-T/\tau_L}$, τ_L is the time constant of the linear EGO sensor and T is the sampling interval, that is, the amount of time per 90 degrees of crank-angle advance. It follows [6] that the combined steady state model of exhaust mixing and linear EGO sensor dynamics is

$$Y = Q_s A_{mix} E \ , \tag{2.15}$$

where

$$Y = \begin{bmatrix} y(8k) \\ y(8k+1) \\ \vdots \\ y(8k+6) \\ y(8k+7) \end{bmatrix}, \ E = \begin{bmatrix} E_5(8k-1) \\ E_6(8k-2) \\ E_7(8k-4) \\ E_8(8k+1) \end{bmatrix},$$

and

$$Q_s = \frac{1-\alpha}{1-\alpha^8}\begin{bmatrix} \alpha^7 & \alpha^6 & \dots & \alpha & 1 \\ \alpha^8 & \alpha^7 & \dots & \alpha^2 & \alpha \\ \vdots & \vdots & \dots & \vdots & \vdots \\ \alpha^{13} & \alpha^{12} & \dots & \alpha^7 & \alpha^6 \\ \alpha^{14} & \alpha^{13} & \dots & \alpha^8 & \alpha^7 \end{bmatrix} + \begin{bmatrix} 0 & 0 & \dots & 0 & 0 \\ 1-\alpha & 0 & \dots & 0 & 0 \\ \vdots & \vdots & \dots & \vdots & \vdots \\ \alpha^5(1-\alpha) & \alpha^4(1-\alpha) & \dots & 0 & 0 \\ \alpha^6(1-\alpha) & \alpha^5(1-\alpha) & \dots & 1-\alpha & 0 \end{bmatrix} .$$

Next, carefully balance each of the cylinders to the stoichiometric A/F, and then off-set each cylinder, succesively, 1 A/F rich and then 1 A/F lean to assess the effect on the A/F at the sensor location. At each condition, let the system reach steady state and then record Y and E over three to ten engine cycles, averaging the components of each vector in order to minimize the impact of noise and cycle to cycle variability in the combustion process. This will provide input A/F vectors $\bar{E} = [\bar{E}^1 ... \bar{E}^8]$ and output A/F vectors $\bar{Z} = [\bar{Y}^1 ... \bar{Y}^8]$, where the overbar represents the averaged value. The least squares solution to (2.15) is then given by

$$A_{mix} = Q_s^{-1}\bar{Z}\bar{E}^T(\bar{E}\bar{E}^T)^{-1} . \tag{2.16}$$

The identified coefficients of A_{mix} should satisfy two conditions: (1) the entries in the matrix lie in the interval [0, 1]; (2) the sum of the entries in any row of the matrix is unity. These conditions correspond to no chemical processes occurring in the exhaust system (which could modify the A/F) between the exhaust valve and the EGO sensor. Inherent nonlinearities in the "linear" EGO sensor or errors in the identification of its time constant often lead to violations of these conditions. In this case, the following fix is suggested. For each row of the matrix, identify the largest negative entry and subtract it from each entry so that all are non-negative; then, scale the row so that its entries sum to one.

2.2.3 Assembling and Validating the State Space Model

A state space model will be used for control law design. The combined dynamics of the A/F system from the fuel scheduler to the EGO sensor is shown in Figure 8. The coefficients $\kappa_1(k), \dots, \kappa_{16}(k)$ arise from constructing a state space representation of (2.11), and thus are directly related to the $a_n(k, j)$. In particular, they are periodic, with period equal to one

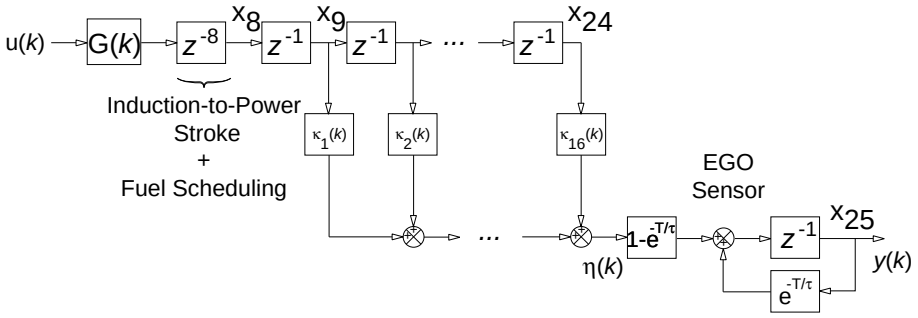

Figure 8: Periodically Time Varying Model of Engine Showing State Variable Assignments.

engine cycle. Figure 9 provides an example of these coefficients for the model identified in [6]. Assigning state variables as indicated, the state space model can be expressed as

k	$\kappa_1(k)$	$\kappa_2(k)$	$\kappa_3(k)$	$\kappa_4(k)$	$\kappa_5(k)$	$\kappa_6(k)$	$\kappa_7(k)$	$\kappa_8(k)$	$\kappa_9(k)$	$\kappa_{10}(k)$	$\kappa_{11}(k)$	$\kappa_{12}(k)$	$\kappa_{13}(k)$	$\kappa_{14}(k)$	$\kappa_{15}(k)$	$\kappa_{16}(k)$
0	0	$a_6(1,1)$	0	$a_7(1,1)$	0	0	$a_8(1,1)$	0	$a_5(1,2)$	0	0	0	0	0	0	0
1	0	0	$a_6(2,1)$	0	$a_7(2,1)$	0	0	$a_8(2,1)$	0	$a_5(2,2)$	0	0	0	0	0	0
2	$a_8(3,0)$	0	0	$a_6(3,1)$	0	$a_7(3,1)$	0	0	0	0	$a_5(3,2)$	0	0	0	0	0
3	0	$a_8(4,0)$	0	0	$a_6(4,1)$	0	$a_7(4,1)$	0	0	0	0	$a_5(4,2)$	0	0	0	0
4	0	0	$a_8(5,0)$	0	0	$a_6(5,1)$	0	$a_7(5,1)$	0	0	0	0	$a_5(5,2)$	0	0	0
5	0	0	0	$a_8(6,0)$	0	0	$a_6(6,1)$	0	$a_7(6,1)$	0	0	0	0	$a_5(6,2)$	0	0
6	0	$a_7(7,0)$	0	0	$a_8(7,0)$	0	0	$a_6(7,1)$	0	0	0	0	0	0	$a_5(7,2)$	0
7	0	0	$a_7(8,0)$	0	0	$a_8(8,0)$	0	0	$a_6(8,1)$	0	0	0	0	0	0	$a_5(8,2)$

Figure 9: Time Dependent Coefficients for Figure (8)

$$\begin{aligned} x(k+1) &= A(k)x(k) + B(k)u(k) \\ y(k) &= C(k)x(k) \ . \end{aligned} \tag{2.17}$$

This is an 8-periodic, SISO system.

For control design, it is convenient to transform this system, via lifting [1, 5], to a linear, time-invariant MIMO system as follows: Let $\bar{x}(k) = x(8k), Y(k) = [y(8k), \ldots, y(8k+7)]^T$, $U(k) = [u(8k), \ldots, u(8k+7)]^T$. Then,

$$\begin{aligned} \bar{x}(k+1) &= \bar{A}\bar{x}(k) + \bar{B}U(k) \ , \\ Y(k) &= \bar{C}\bar{x}(k) + \bar{D}U(k) \end{aligned} \tag{2.18}$$

where: $\bar{A} = A(7)A(6)\cdots A(1)A(0)$,

$$
\begin{aligned}
\bar{B} &= [A(7)A(6)\cdots A(1)B(0) : A(7)A(6)\cdots A(2)B(1) : \cdots : A(7)B(6) : B(7)] \ , \\
\bar{C} &= \begin{bmatrix} C(0) \\ C(1)A(0) \\ \vdots \\ C(6)A(5)\cdots A(0) \\ C(7)A(6)\cdots A(0) \end{bmatrix} \ , \qquad (2.19) \\
\bar{D} &= \begin{bmatrix} 0 & : & 0 & : & \ldots & : & 0 & : & 0 \\ C(1)B(0) & : & 0 & : & \ldots & : & 0 & : & 0 \\ \vdots & : & \vdots & : & \ldots & : & \vdots & : & \vdots \\ C(6)A(5)\cdots A(1)B(0) & : & C(6)A(5)\cdots A(2)B(1) & : & \ldots & : & 0 & : & 0 \\ C(7)A(6)\cdots A(1)B(0) & : & C(7)A(6)\cdots A(2)B(1) & : & \ldots & : & C(7)B(6) & : & 0 \end{bmatrix} .
\end{aligned}
$$

Normally, $\bar{D}$ is identically zero because the time delay separating the input from the sensor is greater than one engine cycle. Since only cylinders 5 through 8 are to be controlled, the $\bar{B}$ and $\bar{D}$ matrices may be reduced by eliminating the columns that correspond to the control variables for cylinders 1 through 4. This results in a system model with 4 inputs and 8 outputs.

Additional data should be taken to validate the identified model of the A/F system. An example of the experimental and modeled response to a unit step input in A/F is shown in Figure 10.

2.2.4 Control Algorithm for ICAFC

The first step is to check the feasibility of independently controlling the A/F in the four cylinders. This will be possible if, and only if[1], the model (2.18), with all of the injector gains set to unity, has 'full rank[2] at dc' (no transmission zeros at 1). To evaluate this, compute the dc-gain of the system

$$G_{dc} = \bar{C}(I - \bar{A})^{-1}\bar{B} + \bar{D}, \qquad (2.20)$$

[1]Since the model is asymptotically stable, it is automatically stabilizable and detectable.

[2]Physically, this corresponds to being able to use constant injector inputs to arbitrarily adjust the A/F in the individual cylinders.

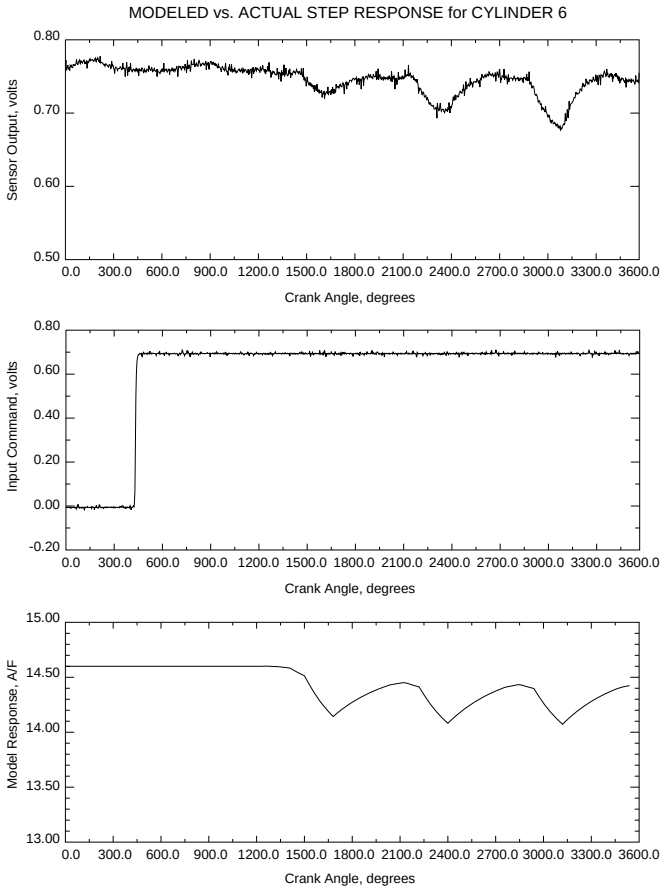

Figure 10: Comparison of Actual and Modeled Step Response for Cylinder Number 6.

and then compute the singular value decomposition (SVD) of G_{dc}. For the regulation problem to be feasible, the ratio of the largest to the fourth largest singular values should be no larger than four to five. If the ratio is too large, then a redesign of the hardware will be necessary before proceeding to the next step [6].

In order to achieve individual set-point control on all cylinders, the system model needs to be augmented with four integrators. This can be done on the input side by

$$\begin{aligned} \bar{x}(k+1) &= \bar{A}\bar{x}(k) + \bar{B}U(k) \\ U(k+1) &= U(k) + V(k) \\ Y(k) &= \bar{C}\bar{x}(k) + \bar{D}U(k) \ , \end{aligned} \tag{2.21}$$

where $V(k)$ is the new control variable, or on the output side. To do the latter, the four

components of Y which are to be regulated to stoichiometry must be selected. One way to do this is to choose four components of Y on the basis of achieving the best numerically conditioned dc-gain matrix when the other four output components are deleted. Denote the resulting reduced output by $\tilde{Y}(k)$. Then, integrators can be added as

$$\begin{aligned} \bar{x}(k+1) &= \bar{A}\bar{x}(k) + \bar{B}U(k) \\ W(k+1) &= W(k) + \Delta\tilde{Y}_m(k) \\ Y(k) &= \bar{C}\bar{x}(k) + \bar{D}U(k) \ , \end{aligned} \tag{2.22}$$

where $\Delta\tilde{Y}_m$ is the error between the measured value of $\tilde{Y}$ and the stoichiometric setpoint.

In either case, it is now very easy to design a stabilizing controller by a host of techniques presented in this handbook. For implementation purposes, the order of the resulting controller can normally be significantly lowered through the use of model reduction methods. Other issues dealing with implementation are discussed in [3], such as, how to incorporate the switching aspect of the sensor into the final controller and how to properly schedule the computed control signals. Specific examples of such controllers eliminating A/F maldistribution are given in [3] and [6].

3 Idle Speed Control

Engine idle is one of the most frequently encountered operating conditions for city driving. The quality of idle speed control (ISC) affects almost every aspect of vehicle performance such as fuel economy, emissions, drivability, etc. The ISC problem has been extensively studied and a comprehensive overview of the subject can be found in [4].

The primary objective for idle speed control is to maintain the engine speed at a desired setpoint in the presence of various load disturbances. The key factors to be considered in its design include:

- **Engine speed setpoint:** To maximize fuel economy, the reference engine speed is scheduled at the minimum that yields acceptable combustion quality, accessory drive

requirements and noise, vibration and harshness (NVH) properties. As the automotive industry strives to reduce fuel consumption by lowering the idle speed, the problems associated with the idle quality (such as allowable speed droop and recovery transient, combustion quality and engine vibration, etc.) tend to be magnified and thus put more stringent requirements on the performance of the control system.

- **Accessory load disturbances:** Typical loads in today's automobile include air conditioning, power steering, power windows, neutral-to-drive shift, alternator loads, etc. Their characteristics and range of operation will determine the complexity of the control design and achievable performance.

- **Control authority and actuator limitations:** The control variables for ISC are air flow (regulated by the throttle or a bypass valve) and spark timing. Other variables, such as A/F, also affect engine operation, but A/F is not considered as a control variable for ISC because it is the primary handle on emissions. The air bypass valve (or throttle) and spark timing are subject to constraints imposed by the hardware itself as well as other engine control design considerations. For example, in order to give spark enough control authority to respond to the load disturbances, it is necessary to retard it from MBT to provide appreciable torque reserve. On the other hand, there is a fuel penalty associated with the retarded spark, which, in theory, can be compensated by the lower idle speed allowed by the increased control authority of spark. The optimal trade-off, however, differs from engine to engine and needs to be evaluated by taking into consideration combustion quality and the ignition hardware constraints (the physical time required for arming the coil and firing the next spark imposes a limitation on the allowable spark advance increase between two consecutive events).

- **Available measurement:** Typically, only engine speed is used for ISC feedback. Manifold absolute pressure (MAP), or inferred MAP, is also used in some designs. Ac-

cessory load sensors (such as the air conditioning switch, neutral-to-drive shift switch, power steering pressure sensor, etc.) are installed in many vehicles to provide information on load disturbances for feedforward control.

- **Variations in engine characteristics over the entire operating range:** The ISC design has to consider different operational and environmental conditions such as temperature, altitude, etc. To meet the performance objectives for a large fleet of vehicles throughout their entire engine life, the control system has to be robust enough to incorporate changes in the plant dynamics due to aging and unit-to-unit variability.

The selection of desired engine setpoint and spark retard is a sophisticated design trade-off process and is beyond the scope of this article. The control problem addressed here is the speed tracking problem which can be formally stated as: *For a given desired engine speed setpoint, design a controller which, based on the measured engine speed, generates commands for the air bypass valve and spark timing to minimize engine speed variations from the setpoint in the presence of load disturbances.* A schematic control system diagram is shown in Figure 11.

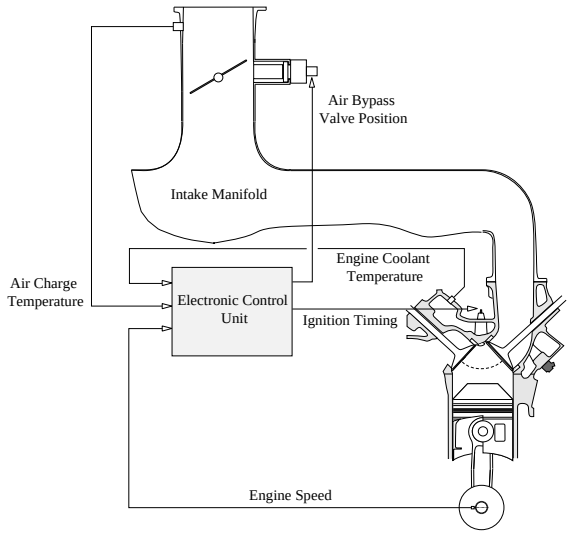

Figure 11: Sensor-Actuator Configuration for ISC.

3.1 Engine Models for ISC

An engine model which encompasses the most important characteristics and dynamics of engine idle operation is given in Figure 12. It uses the model structure developed in [7] and consists of the actuator characteristics, manifold filling dynamics, engine pumping characteristics, intake-to-power stroke delay, torque characteristics and engine rotational dynamics (EGR is not considered at idle). The assumption of sonic flow through the throttle, generally

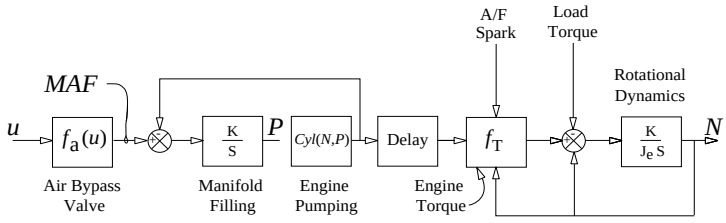

Figure 12: Nonlinear Engine Model.

satisfied at idle, has led to a much simplified model where the air flow across the throttle is only a function of the throttle position. The differential equations describing the overall dynamics are given by:

$$\begin{aligned} MAF &= f_a(u) \\ \dot{P} &= K_m(MAF - \dot{m}) \\ \dot{m} &= Cyl(N, P) \\ J_e\dot{N} &= T_q - T_L, \\ T_q(t) &= f_T(\dot{m}(t-\sigma), N(t), r(t-\sigma), \delta(t)) \end{aligned} \tag{3.23}$$

where:
- u: duty cycle for the air-bypass valve
- r: A/F ratio
- δ: spark timing in terms of crank angle degrees before top dead center
- T_L: load torque

J_e and K_m in (3.23) are two engine dependent constants, where J_e represents the engine rotational inertia, and K_m is a function of the gas constant, air temperature, manifold volume, etc. Both J_e and K_m can be determined from engine design specifications and given nominal operating conditions. The time delay σ in the engine model equals approximately

180 degrees of crank-angle advance, and thus is a speed dependent parameter. This is one reason that models for ISC often use crank angle instead of time as the independent variable. Additionally, most engine control activities are event driven and synchronized with crank position; the use of $\frac{dM}{d\theta}$ and $\frac{dP}{d\theta}$ instead of $\frac{dM}{dt}, \frac{dP}{dt}$ respectively tends to have a linearizing effect on the pumping and torque generation blocks.

Performing a standard linearization procedure results in the linear model shown in Figure 13, with inputs $\Delta u, \Delta\delta, \Delta T_L$ (the change of the bypass valve duty cycle, spark, and load torque from their nominal values, respectively) and output ΔN (the deviation of the idle speed from the setpoint). The time delay in the continuous-time feedback loop usually complicates the control design and analysis tasks. In a discrete-time representation, however,

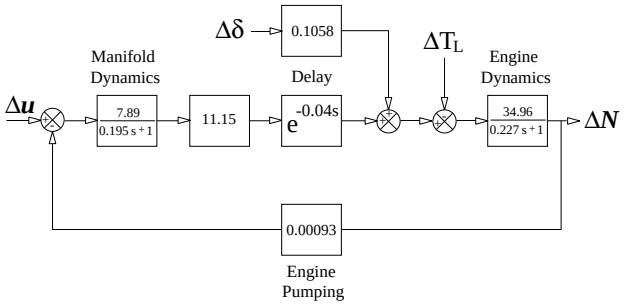

Figure 13: Linearized Model for Typical 8-Cylinder Engine.

the time delay in Figure 13 corresponds to a rational transfer function z^{-n} where n is an integer that depends on the sampling scheme and the number of cylinders. It is generally more convenient to accomplish the controller design using a discrete-time model.

3.2 Determining Model Parameters

In the engine model of (3.23), the nonlinear algebraic functions f_a, f_T, Cyl describe characteristics of the air bypass valve, torque generation and engine pumping blocks. These functions can be obtained by regressing engine dynamometer test data, using least squares or other curve fitting algorithms. The torque generation function is developed on the engine dynamometer by individually sweeping ignition timing, A/F and mass flow rate (regulated

by throttle or air bypass valve position) over their expected values across the idle operating speed range. For a typical eight cylinder engine, the torque regression is given by

$$\begin{aligned} T_q &= f_T(MAF, N, r, \delta) \\ &= -28.198 + 128.38MAF - 0.196N + 13.845r - 0.306\delta - 5.669MAF^2 \\ &\quad +7.39 \times 10^{-5}N^2 - 0.6257r^2 - 0.0257\delta^2 - 0.0379MAF \cdot N + 0.2843MAF \cdot r \\ &\quad -0.2483MAF \cdot \delta - 0.00059N \cdot r + 0.00067N \cdot \delta + 0.0931r \cdot \delta \end{aligned}$$

The steady-state speed-torque relation to spark advance is illustrated in Figure 14.

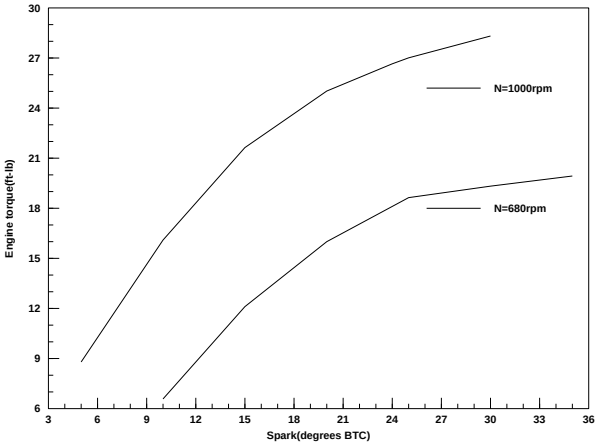

Figure 14: Spark-Torque Relation for Different Engine Speeds (with A/F=14.64).

For choked (i.e., sonic) flow, the bypass valve's static relationship is developed simply by exercising the actuator over its operating envelope and measuring mass airflow using a hot wire anemometer, or volume flow by measuring the pressure drop across a calibrated laminar flow element. The dynamic elements in the linearized idle speed model can be obtained by linearizing the model in Subsection 2.1, or they can be estimated by evaluating (small) step response data from a dynamometer. In particular, the intake manifold time constant can be validated by constant speed, sonic flow throttle step tests, using a sufficiently high bandwidth sensor to measure manifold pressure.

3.3 ISC Controller Design

The ISC problem lends itself to the application of various control design techniques. Many different design methodologies, ranging from classical (such as PID) to modern (such as LQG, H_∞, adaptive, etc) and non-conventional (such as neural networks and fuzzy logic) designs have been discussed and implemented [4]. The mathematical models described in Section 3.1 and commercially available software tools can be used to design different control strategies, depending on the implementor's preference and experience. A general ISC system with both feedforward and feedback components is shown in the block diagram of Figure 15.

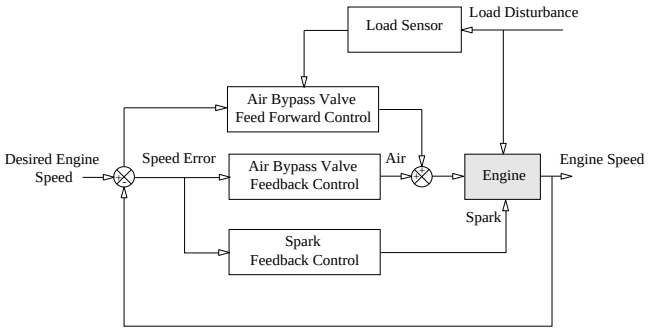

Figure 15: General ISC System with Feedforward and Feedback Elements.

3.3.1 Feedforward control design

Feedforward control is considered as an effective mechanism to reject load disturbances, especially for small engines. When a disturbance is measured (most disturbance sensors used in vehicles are on-off type), control signals can be generated in an attempt to counteract its effect. A typical ISC strategy has feedforward only for the air bypass valve control, and the feedforward is designed based on static engine mapping data. For example, if an air conditioning (AC) switch sensor is installed, an extra amount of air will be scheduled to prevent engine speed droop when the AC compressor is engaged. The amount of feedforward control can be determined as follows: At the steady state, since $\dot{P}, \dot{N} \approx 0$, the available engine torque to balance the load torque is related to the mass air flow and engine speed through:

$$T_q = f_T(MAF, N, r, \delta).$$

By estimating the load torque presented to the engine by the measured disturbance, one can calculate, for fixed A/F ratio and spark, the amount of air that is needed to maintain the engine speed at the fixed setpoint. The feedforward control can be applied either as a multiplier or an adder to the control signal.

Feedforward control introduces extra cost due to the added sensor and software complexity, and thus it should be used only when necessary. Most importantly, it should not be used to replace the role of feedback in rejecting disturbances, since it also does not address the problems of operating condition variations, miscalibration, etc.

3.3.2 Feedback design

Feedback design for ISC can be pursued in many different ways. Two philosophically different approaches are used in developing the control strategy: One is the single-input single-output (SISO) approach which treats the air and spark control as separate entities and designs one loop at a time. When the SISO approach is used, the natural separation of time scale in the air and spark dynamics (spark has a fast response compared to air flow, which has a time lag due to the manifold dynamics and intake-to-power delay) suggests that the spark control be closed first as an inner loop. Then the air control, as an outer loop, is designed by including the spark feedback as part of the plant dynamics. Another approach is to treat the ISC as a multi-input single-output or, when the manifold pressure is to be controlled, a multi-input multi-output (MIMO) problem. Many control strategies, such as LQ-optimal control and H_∞ have been developed within the MIMO framework. This approach generally leads to a coordinated air and spark control strategy and improved performance.

Despite the rich literature on ISC featuring different control design methodologies, PID control in combination with static feedforward design is still viewed as the control structure of choice in the automotive industry. In many cases, controllers designed using advanced theory, such as H_∞ and LQR, are ultimately implemented in the PID format to reduce complexity and to append engineering content to design parameters. A typical production

ISC feedback strategy has a PID for the air bypass valve (or throttle) control, and a simple proportional feedback for the spark control. This control configuration is dictated by the following requirements: (1) At steady state, the spark should return to its nominal value independent of the load disturbances; (2) Zero steady-state error has to be attained for step disturbances.

3.4 Calibration of ISC

Control system development in the automotive industry has been traditionally an empirical process with heavy reliance on manual tuning. As engine control systems have become more complex because of increased functionality, the old-fashioned trial-and-error approach has proved inadequate to achieve optimum performance for interactively connected systems. The trends in today's automotive control system development are in favor of more model-based design and systematic calibration. Tools introduced for performing systematic in-vehicle calibration include dynamic optimization packages which are used to search for optimal parameters based on a large amount of vehicle data, and controller fine-tuning techniques. Given the reality that most ISC strategies implemented in vehicles are of PID type, we discuss two PID tuning approaches that have proved effective in ISC calibration.

The first method is based on the sensitivity functions of the engine speed with respect to the controller parameters. Let K be a generic controller parameter (possibly vector valued) and suppose that we want to minimize a performance cost function $J(\Delta N)$ (a commonly used function for J is $J = (\Delta N)^2$) by adjusting K. Viewing ΔN as a function of K and noting that $\frac{\partial \Delta N}{\partial K} = \frac{\partial N}{\partial K}$, we have

$$J(K + \Delta K) \approx J(K) + 2\Delta N \frac{\partial N}{\partial K}\Delta K + (\Delta K)^\top \left(\frac{\partial N}{\partial K}\right)^\top \frac{\partial N}{\partial K}\Delta K.$$

According to Newton's method, ΔK which minimizes J is given by

$$\Delta K = -\left[\left(\frac{\partial N}{\partial K}\right)^\top \frac{\partial N}{\partial K}\right]^{-1} \left(\frac{\partial N}{\partial K}\right)^\top \Delta N. \tag{3.24}$$

By measuring the sensitivity function $\frac{\partial N}{\partial K}$, we can use a simple gradient method or (3.24) to iteratively minimize the cost function J. The controller gains for the air and spark loops can be adjusted simultaneously. The advantages of the method are that the sensitivity functions are easy to generate. For the ISC calibration, the sensitivity functions of N with respect to PID controller parameters can be obtained by measuring the signal at the sensitivity points, as illustrated in Figure 16.

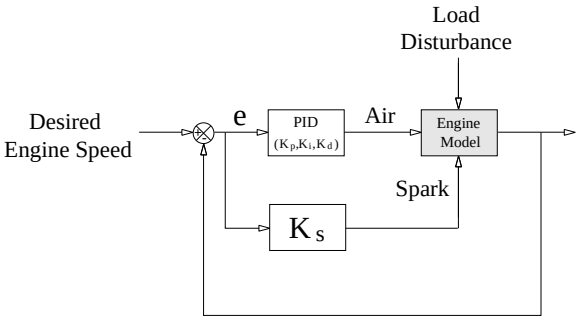

PID control for ISC

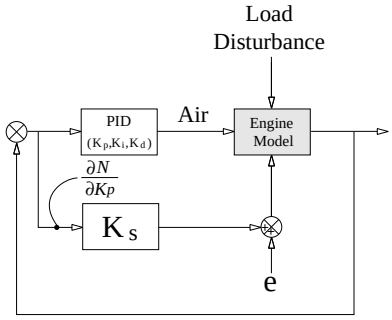

Sensitivity points for proportional spark-loop control

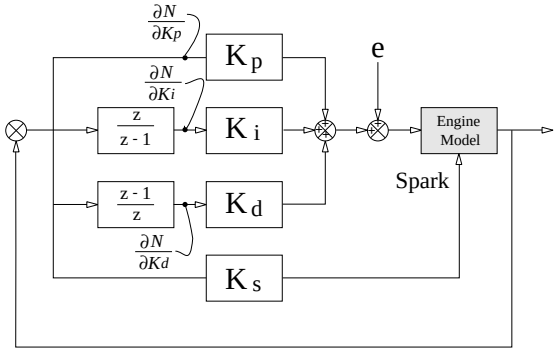

Sensitivity points for PID air-loop control

Figure 16: Sensitivity Points for Calibrating PID Idle Speed Controller.

It should be pointed out that this off-line tuning principle can be used to develop an on-line adaptive PID control scheme (referred to as the M.I.T. rule in the adaptive control literature). The sensitivity function method can also be used to investigate the robustness of the ISC system with respect to key plant parameters by evaluating $\frac{\partial N}{\partial K_p}$ where K_p is the plant parameter vector.

The second method is the well-known Ziegler-Nichols PID tuning method. It gives a set of heuristic rules for selecting the optimal PID gains. For the ISC applications, modifications have to be introduced to accommodate the time delay and other constraints. Generally, the Ziegler-Nichols sensitivity method is used to calibrate the PID air feedback loop after the proportional gain for the spark is fixed.

4 Acknowledgment

The authors would like to acknowledge their many colleagues at Ford and the University of Michigan who contributed to the work described in this article, with special thanks to Dr. Paul Moraal of Ford.

References

[1] K.L. Buescher, *Representation, Analysis, and Design of Multirate Discrete-Time Control Systems*, MS Thesis, Department of Electrical and Computer Engineering, University of Illinois, Urbana-Champaign, 1988.

[2] J.W. Grizzle, J.A. Cook and W.P. Milam, "Improved cylinder air charge estimation for transient air fuel ratio control", *Proc. 1994 American Control Conference*, Baltimore, MD, June, 1994, pp. 1568-1573.

[3] J.W. Grizzle, K.L. Dobbins and J.A. Cook, "Individual cylinder air fuel ratio control with a single EGO sensor", *IEEE Trans. Vehicular Technology*, Vol. 40, No. 1, February, 1991, pp. 280-286.

[4] D. Hrovat and W. F. Powers, "Modeling and Control of Automotive Power Trains," *Control and Dynamic Systems*, Vol. 37, Academic Press, 1990, pp. 33-64.

[5] P.P. Khargonekar, K. Poolla, and A. Tannenbaum, "Robust Control of Linear Time-Invariant Plants Using Periodic Compensation, *IEEE Trans. Auto. Cont.*, Vol AC-30, No. 11, 1985, pp. 1088-1096.

[6] P.E. Moraal, J.A. Cook, and J.W. Grizzle, "Single Sensor Individual Cylinder Air-Fuel Ratio Control of an Eight Cylinder Engine with Exhaust Gas Mixing", *Proc. 1993 American Control Conference*, San Francisco, CA, June, 1993, pp. 1761-1767.

[7] B. K. Powell and J. A. Cook, "Nonlinear Low Frequency Phenomenological Engine Modeling and Analysis," *Proc. 1987 American Control Conference*, Minneapolis, MN, June, pp. 332-340.

[8] W.F. Powers, "Customers and Controls", *IEEE Control Systems Magazine*, Vol. 13, No. 1, February, 1993, pp. 10-14.

[9] M.A. Shulman and D.R. Hamburg, "Non-ideal Properties of Z_rO_2 and T_iO_2 Exhaust Gas Oxygen Sensors," *SAE Technical Paper Series*, No. 800018, 1980.

[10] C. F. Taylor, "The Internal Combustion Engine in Theory and Practice, Volume 1: Thermodynamics, Fluid Flow, Performance," MIT Press, 1980.